Wideband Frequency-Domain Characterization of High-Impedance Probes

Uwe Arz, Howard C. Reader[1], Pavel Kabos, Dylan F. Williams

National Institute of Standards and Technology
325 Broadway, Boulder, CO 80305, USA
Phone: [+1] 303.497.4254 Fax: [+1] 303.497.3970 E-mail: uarz@boulder.nist.gov

***Abstract*- We investigated the broadband microwave properties of high-impedance probes designed for on-wafer waveform measurements. We show that the standard two-tier characterization method fails. We introduce two new methods of characterization, both of which yield equivalent results.**

INTRODUCTION

In this paper we introduce two methods of characterizing commercially available high-impedance probes. The probes we study are similar to standard hand-held oscilloscope probes used to measure digital waveforms on printed circuit boards. However, with the advent of high-speed digital circuits and the rapid developments in the telecommunications industry, these traditional handheld probes are no longer adequate measurement tools. Internal-node testing of integrated microwave and digital circuits is driving the demand for accurate on-wafer non-invasive high-bandwidth probing. For example, micromachined microwave and photoconductive sampling probes, with a possible bandwidth in excess of 100 GHz, are current topics of research [1,2].

Here, we investigate commercial high-impedance probes mounted on micropositioners that can touch down on small contact pads on an integrated circuit. Like their hand-held counterparts, these passive probes have a small series resistor embedded in the tip to reduce invasiveness. The characterization methods we develop in this paper may serve as a first step for correcting both time-domain and frequency-domain measurements performed with these probes. We also investigate the limitations of these probes for measuring scattering parameters.

---

[1]H.C. Reader is on sabbatical from the University of Stellenbosch, South Africa.

STANDARD PROBE CHARACTERIZATION PROCEDURE

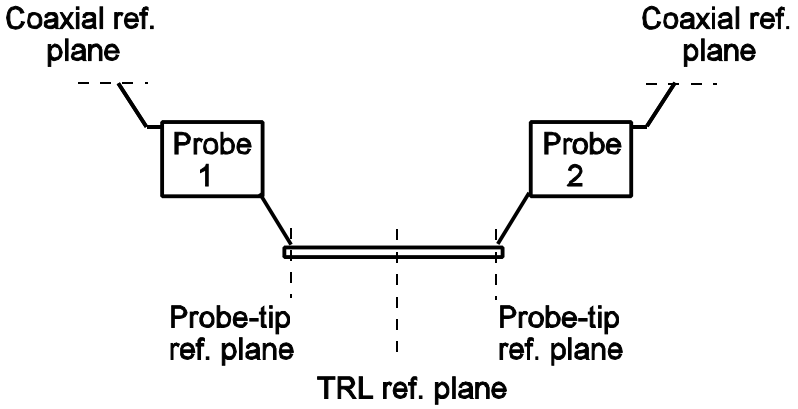

Fig. 1: Experimental setup.

Bauer and Penfield [3] presented what has now become the standard two-tier fixture characterization scheme. The method begins with a first-tier scattering-parameter calibration at a reference plane outside the fixture. Bauer and Penfield then used this calibration to measure the S-parameters of the fixture with several known artifacts placed inside it. Each measurement yields new information about the fixture. Bauer and Penfield showed how to make optimum use of the measurements to completely describe the electrical characteristics of the fixture.

We first applied this standard method to derive the electrical characteristics of our high-impedance probe. The measurement configuration pertinent to our discussion is depicted in Fig. 1. We began by performing a first-tier sliding-load Short-Open-Load-Thru (SOLT) vector network analyzer calibration at the coaxial reference planes in the figure. Between these planes, we then connected a standard 50 Ω ground-signal-ground (GSG) probe on the left (Probe 1), and the high-impedance probe (HIP) under investigation on the right (Probe 2). With these probes we contacted coplanar waveguide (CPW) artifacts fabricated on a low-loss GaAs substrate and performed on-wafer measurements of their scattering parameters. The artifacts included 20.195 mm, 7.065 mm, 3.7 mm, 2.635 mm long lines, a 0.5 mm long Thru line, and a symmetric reflect. Then, we performed a multiline Thru-Reflect-Line (TRL) calibration [4], which sets the TRL reference plane in the middle of the CPW Thru line. Finally, we moved the reference plane of the calibration back to the probe tip reference plane, as indicated in Fig. 1. This is commonly referred to as a second-tier calibration.

This second-tier calibration maps measurements at the initial coaxial calibration reference plane to the final probe-tip reference plane on the wafer by means of two electrical two-ports, which are often called “error boxes”. In this instance, the error box on the left describes the electrical characteristics of the GSG probe, while the error box on the right determines the S-parameters of the high-impedance probe.

The dashed lines in Figs. 2 to 7 show the results of this conventional two-tier procedure. This procedure clearly fails to accurately determine the S-parameters of the high-impedance probe. This is evident from the noise in the S_{11} and S_{21} measurements, and the non-physical gain in the magnitude of S_{11}.

NEW PROBE CHARACTERIZATION PROCEDURES

Both of our new characterization procedures begin with the standard two-tier characterization of two 50 Ω GSG probes, one mounted on the left as Probe 1, the other on the right as Probe 2. For these typical microwave probes, the standard two-tier procedure worked well, yielding the S-parameters of both the GSG-

probes and the CPW line artifacts. These S-parameter descriptions of GSG-Probe 1, GSG-Probe 2 and the lines, Lx, are needed for the following stages.

Method A: Coaxial 1st-Tier Calibration

In our first procedure, we replace the GSG probe on the right side with the high-impedance probe we wish to characterize, and then contact one of the CPW line standards. At the coaxial reference planes, we then measure the SOLT-corrected S-parameters of the combined two probes and line chain. This chain can be described as a cascade of the transmission matrices (transformed from the S-parameters) representing the corresponding devices between the coaxial reference planes. That is, $\boldsymbol{T}_{total}^{SOLT} = \boldsymbol{T}_{GSG-Probe1} \cdot \boldsymbol{T}_{Lx} \cdot \boldsymbol{T}_{HIP-Probe2}$, where $\boldsymbol{T}_{total}^{SOLT}$ is the transmission matrix corresponding to the entire chain. $\boldsymbol{T}_{GSG-Probe1}$ is the transmission matrix of the GSG-probe on the left, and $\boldsymbol{T}_{Lx}$ is the transmission matrix of the line standard, both of which are derived from the earlier standard two-tier characterization step with both GSG-probes mounted. $\boldsymbol{T}_{HIP-Probe2}$ is the transmission matrix of the high-impedance probe on the right that we wish to characterize. We then determine $\boldsymbol{T}_{HIP-Probe2}$ using $\boldsymbol{T}_{HIP-Probe2} = [\boldsymbol{T}_{GSG-Probe1} \cdot \boldsymbol{T}_{Lx}]^{-1} \cdot \boldsymbol{T}_{total}^{SOLT}$.

We repeated the procedure for all the CPW-line lengths available and averaged the results to improve the characterization of the high-impedance probe. The results of this procedure are shown as solid lines with squares in Figs. 2 to 7. These results are much better behaved than those of the standard two-tier scheme.

Method B: On-Wafer First-Tier Calibration

In contrast to Method A, where only the GSG-Probe 1 S-parameters are needed, Method B requires that the GSG probes on *both* port 1 and 2 have already been characterized, as described in the first paragraph of this section. This will allow us to move the reference planes of our measurements from on-wafer locations at the probe tips to the coaxial ports.

We start by performing a first-tier on-wafer multiline TRL calibration with the two pre-characterized GSG-Probe 1 and GSG-Probe 2 mounted. This on-wafer calibration is used to correct all subsequent measurements.

We now replace the GSG-Probe 2 on the right with the high-impedance probe and take measurements of the on-wafer CPW line standards, calibrating the measurement data with the on-wafer multiline TRL calibration. The transmission matrix $\boldsymbol{T}_{total}^{MTRL}$ determined by this calibration is related to the transmission matrix $\boldsymbol{T}_{total}^{SOLT}$ of a measurement corrected at the coaxial reference planes by $\boldsymbol{T}_{total}^{MTRL} = \boldsymbol{T}_{GSG-Probe1}^{-1} \cdot \boldsymbol{T}_{total}^{SOLT} \cdot \boldsymbol{T}_{GSG-Probe2}^{-1}$.

We are thus able to move the measurement reference planes back to the coaxial ports with $\boldsymbol{T}_{total}^{SOLT} = [\boldsymbol{T}_{GSG-Probe1}^{-1}]^{-1} \cdot \boldsymbol{T}_{total}^{MTRL} \cdot [\boldsymbol{T}_{GSG-Probe2}^{-1}]^{-1}$, which can be interpreted as deembedding the inverse error boxes of the GSG probes from the on-wafer measurements. This “inverse-deembedding” can be considered equivalent to calibrating the measurements with a SOLT procedure at the coaxial reference planes.

Since we are now able to correct measurements to the coaxial reference plane, we can apply the procedural steps of method A. We again derived the final high-impedance probe characterization by averaging results obtained from the different CPW line lengths.

The results of this procedure are shown as solid lines with circles in Figs. 2 to 7, and almost coincide with the results obtained from Method A, thereby proving the consistency of both new methods. The results obtained from methods A and B exhibit significantly less noise than the standard two-tier method, thereby illustrating their superiority.

The main advantage of Method B over Method A is that, once the GSG probes have been characterized with the standard two-tier procedure, the high-impedance probe can be entirely characterized by means of on-wafer measurements. No additional coaxial measurements are necessary. Method B also requires fewer disconnections of the measurement cables.

PROPERTIES OF THE HIGH-IMPEDANCE PROBE

The results obtained with methods A and B shown in Figs. 2-7 demonstrate the properties of the high-impedance probe. The high-impedance probe we used in our experiments had a built-in 950 Ω resistor at the probe tip, yielding a transmission parameter of aproximately -20dB. Due to the relative length of line between the probe tip and the coaxial reference plane the phase of S_{21} changes rapidly. Figure 5 shows that the difference between the phases measured with methods A and B is negligible over the entire frequency band. Figure 5 also shows the unwrapped phase of S_{21} measured with methods A and B after subtracting a constant delay of 0.66 ns, which is derived from a linear fit of the low-frequency phase characteristics.

The high S_{11} and S_{22} magnitudes are a consequence of the resistor in the probe tip. The large difference between the phases of S_{11} and S_{22} occurred because the probe resistor was positioned close to the probe tip (port 1 reference plane), whereas the reference plane of port 2 was separated from the probe resistor by a length of semi-rigid coaxial line and a length of coax inside the probe.

Based on the consistency of the results from methods A and B, we can envision correction procedures for both frequency- and time-domain measurements. In the next section, we investigate frequency-domain S-parameter measurements.

MEASUREMENTS USING THE HIGH-IMPEDANCE PROBE

The high-impedance probe under investigation is designed for waveform measurements inside integrated circuits. Nevertheless, we investigated the capabilities of the high-impedance probe to perform frequency-domain measurements, despite the fact that this probe was never intended for this purpose.

We began our investigation by measuring a 19 mm long CPW line and a resistive attenuator using GSG probes on both ports together with a first-tier multiline TRL calibration. These measurements are labeled MTRL-GSG-GSG in Figs. 8 to 13. Because we used low-loss microwave probes and a well-established calibration method, we expected these measurements to be accurate. In fact, they are well-behaved over the entire frequency range up to 40 GHz, and will serve as a reference to which we compare our other results.

With the GSG probe on port 1 and the high-impedance probe on port 2 we next measured the 19 mm CPW line and the resistive attenuator with respect to the coaxial reference plane. We then used the S-parameters

describing the GSG and high-impedance probes determined from Method A to deembed the results to the on-wafer probe-tip reference plane. These are labeled SOLT-GSG-HIP in Figs. 8 to 13. (Since the quality of the high-impedance characterization using methods A and B does not differ significantly, we do not present S-parameter results for method B.)

Figures 8 and 9 demonstrate that S_{11} can be reasonably well measured using the deembedding technique (SOLT-GSG-HIP). However, the method is very sensitive to configurational issues as can be seen from resonances appearing at several distinct frequencies. For instance, the resonance at approximately 2 GHz can be attributed to a common-mode current path around the wafer carrying the test structures.

Figures 10 and 11 indicate that S_{21} cannot be accurately extracted. The deviation from the reference result is a good indication of the level of accuracy that can be obtained. Figures 12 and 13 show that no reasonable measurements of S_{22} can be obtained.

Finally, we also tried correcting our measurements with a direct one-tier multiline TRL calibration procedure, performed with a GSG probe on port 1 and the high-impedance probe on port 2. The corresponding results are labeled as MTRL-GSG-HIP. One consequence of this first-tier calibration procedure is that it is impossible to derive a probe characterization.

The figures show that, in general, the direct TRL approach (MTRL-GSG-HIP) is inferior to the deembedding technique (SOLT-GSG-HIP), but neither method is comparable to the reference results obtained with both GSG probes.

CONCLUSIONS

We showed that the standard two-tier characterization scheme fails for high-impedance probes. We introduced two new methods capable of determining the electrical properties of high-impedance probes. From the results that we presented, we conclude that high-impedance probes have obvious limitations for frequency-domain S-parameter measurement. However, we expect that our probe characterization will be useful in correcting on-wafer time-domain waveform measurements.

REFERENCES

[1] G. David, T.-Y. Yun, M.H. Crites, J.F. Whitaker, T.R. Weatherford, K. Jobe, S. Meyer, M.J. Bustamante, B. Goyette, S. Thomas III, and K.R. Elliott, “Absolute Potential Measurements Inside Microwave Digital IC’s Using a Micromachined Photoconductive Sampling Probe”, *IEEE Trans. Microwave Theory Tech.*, vol. 46, no. 12, pp. 2330-2337, Dec. 1998.

[2] D.W. van der Weide, “Localized Picosecond Resolution With a Near-field Microwave/Scanning-force Microscope”, *Applied Phys. Lett*, vol. 70, no. 6, pp. 677-679, Feb. 1997.

[3] R.F. Bauer, and P. Penfield, “De-Embedding and Unterminating”, *IEEE Trans. Microwave Theory Tech.*, vol. MTT-22, no. 3, pp. 282-288, March 1974.

[4] R.B. Marks, “A Multiline Method of Network Analyzer Calibration”, *IEEE Trans. Microwave Theory Tech.*, vol. MTT-39, no. 7, pp. 1205-1215, July 1991.

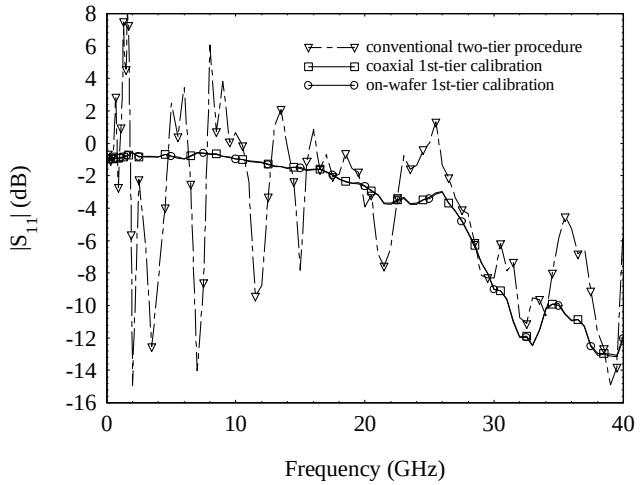

Fig. 2. Magnitude $|S_{11}|$ of high-impedance probe.

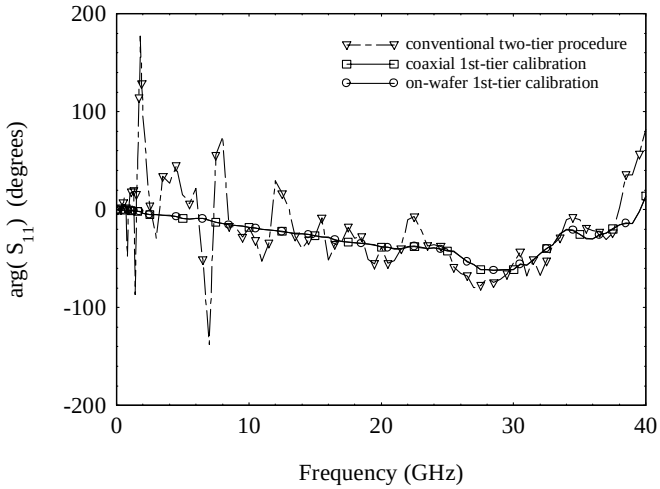

Fig. 3. Phase $\arg(S_{11})$ of high-impedance probe.

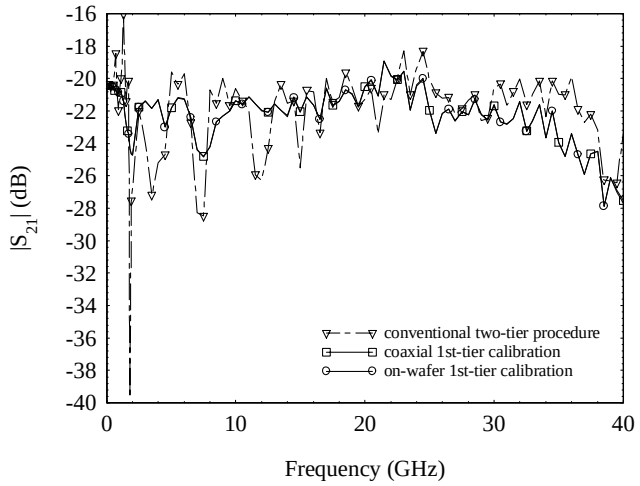

Fig. 4. Magnitude $|S_{21}|$ of high-impedance probe.

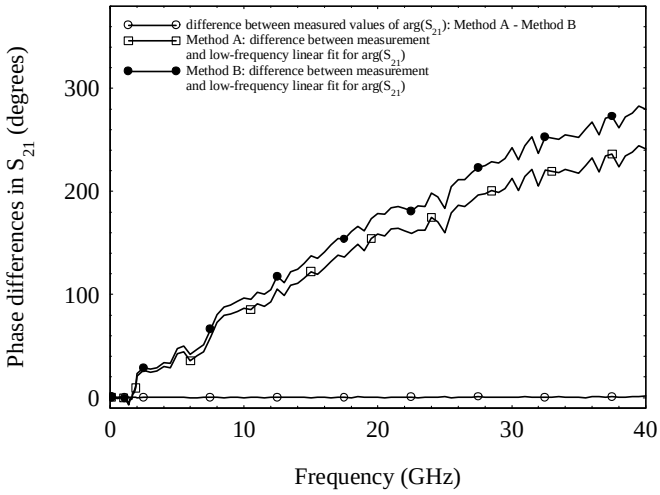

Fig. 5. Properties of $\arg(S_{21})$ of high-impedance probe.

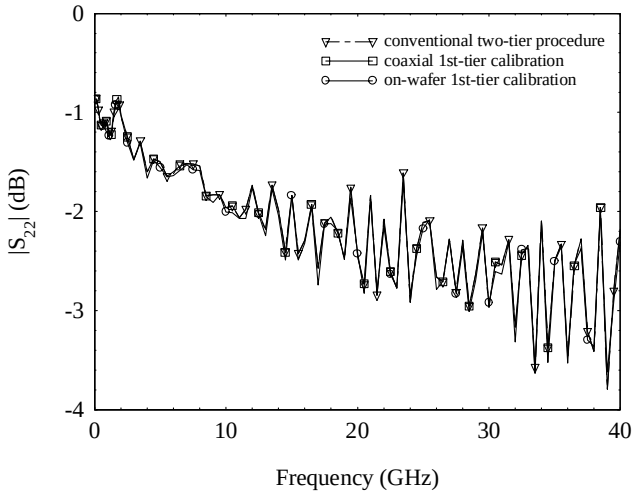

Fig. 6. Magnitude $|S_{22}|$ of high-impedance probe.

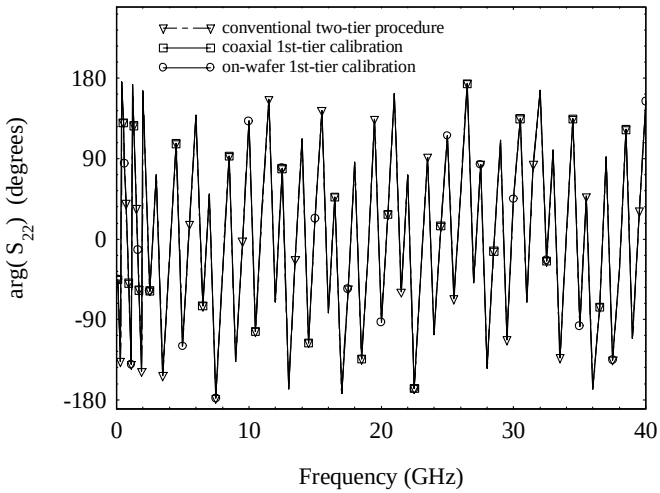

Fig. 7. Phase $\arg(S_{22})$ of high-impedance probe.

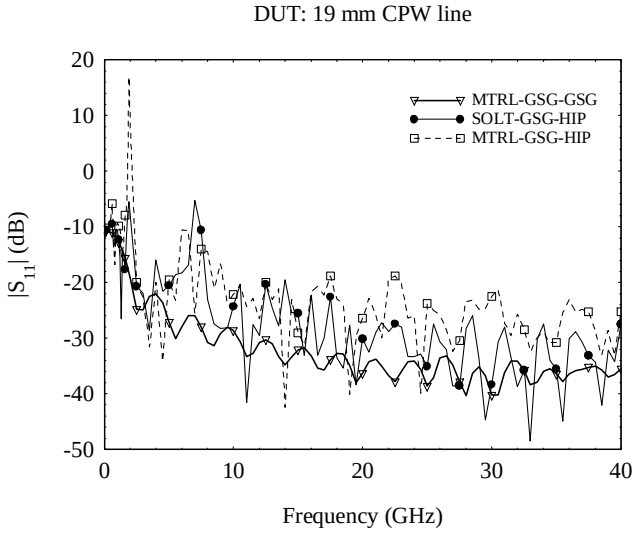

Fig. 8. $|S_{11}|$ measurement of 19 mm CPW line.

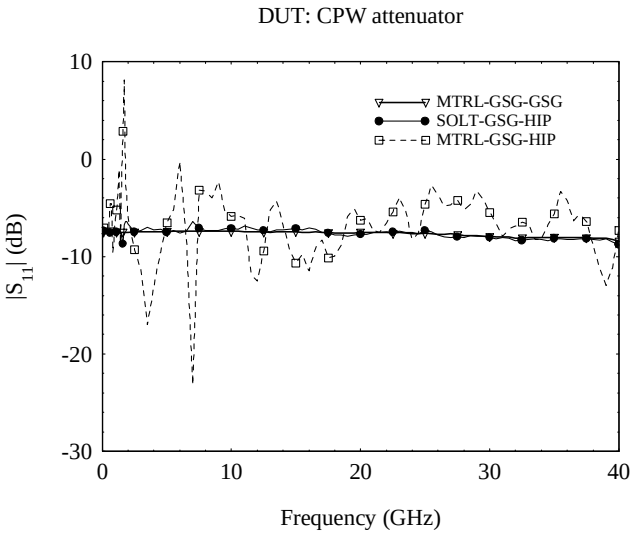

Fig. 9. $|S_{11}|$ measurement of CPW attenuator.

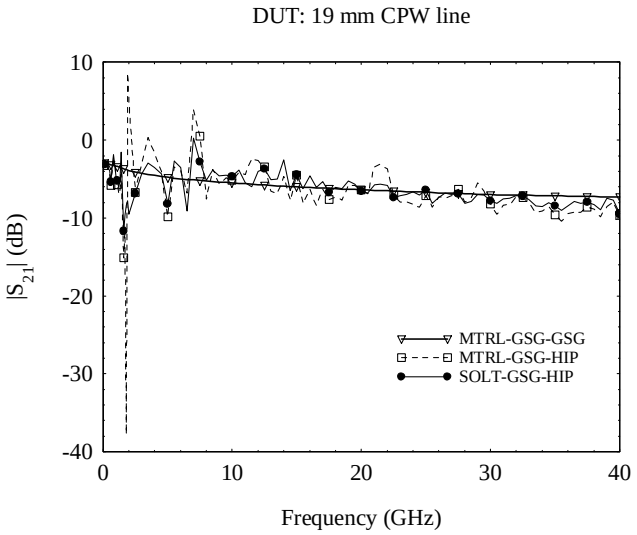

Fig.10. $|S_{21}|$ measurement of 19 mm CPW line.

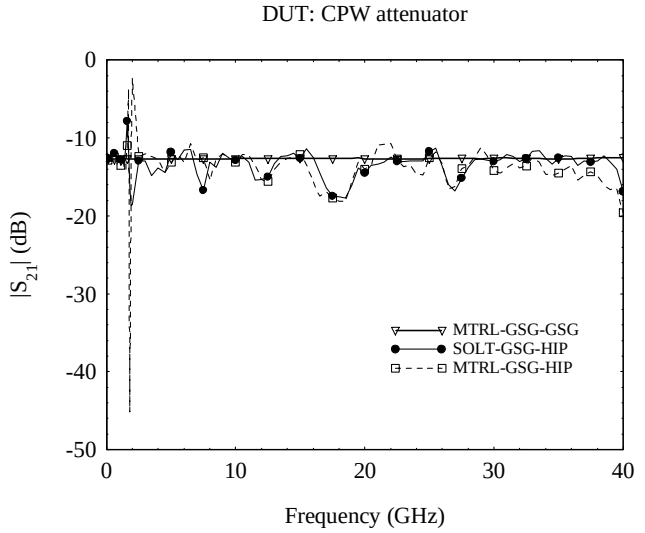

Fig. 11. $|S_{21}|$ measurement of CPW attenuator.

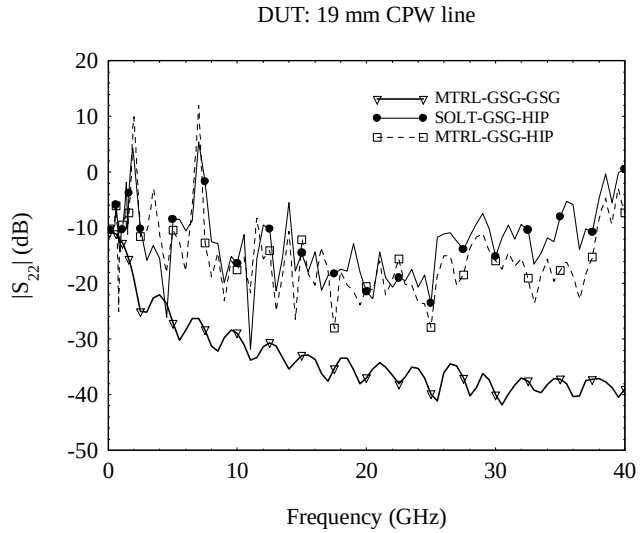

Fig. 12. $|S_{22}|$ measurement of 19 mm CPW line.

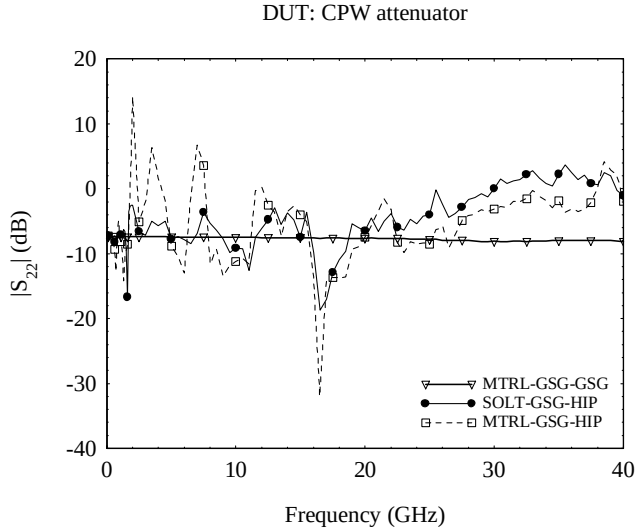

Fig. 13. $|S_{22}|$ measurement of CPW attenuator.